

Available online at www.sciencedirect.com**ScienceDirect**journal homepage: www.elsevier.com/locate/issn/15375110**Research Paper**

High-resolution multispectral imagery and LiDAR point cloud fusion for the discrimination and biophysical characterisation of vegetable crops at different levels of nitrogen



Rama Rao Nidamanuri ^{a,*}, Reji Jayakumari ^a, Anandakumar M. Ramiya ^a, Thomas Astor ^b, Michael Wachendorf ^b, Andreas Buerkert ^c

^a Department of Earth and Space Sciences, Indian Institute of Space Science and Technology, Department of Space, Government of India, Thiruvananthapuram 695 547, India

^b Grassland Science and Renewable Plant Resources, Organic Agricultural Sciences, Universität Kassel, D-37213 Witzenhausen, Germany

^c Organic Plant Production and Agroecosystems Research in the Tropic and Subtropics, Organic Agricultural Sciences, Universität Kassel, D-37213 Witzenhausen, Germany

ARTICLE INFO**Article history:**

Received 7 October 2021

Received in revised form

13 August 2022

Accepted 19 August 2022

Published online 10 September 2022

Keywords:

Precision agriculture

Supervised crop classification

Crown area and biomass

Data fusion

LiDAR point cloud

Biophysical characterisation

High-resolution remote sensing data has expanded the scope, precision, and scale of remote sensing applications in agriculture. Availability of spatial information at actionable field units is vital for using remote sensing data in agriculture. Crop discrimination and biophysical characterisation sensitive to nutrient levels have not been addressed at the patch level. This work investigates the synergistic application of high-resolution satellite imagery and terrestrial LiDAR point cloud for object-level discrimination and biophysical characterisation of a few crops at different nitrogen (N) levels. To this end, cabbage, eggplant, and tomato at three levels of N were grown on the experimental fields of the University of Agricultural Sciences, Bengaluru, India, in 2017. Fusing the multispectral imagery (WorldView-III) and LiDAR point cloud (terrestrial laser scanner) at the feature level, object-level supervised classification and estimation of two critical biophysical parameters (crown area and biomass) were performed using the support vector machine (SVM) and Random Forests (RF) algorithms with reference to different N levels. Results suggest discrimination of vegetable crops with high accuracy (92%), about 20% higher than the individual sensors, from the fused imagery sensitive to N levels. The quality of retrievals indicates a contrasting pattern wherein the accuracy of the crown area is high with the LiDAR point cloud at various N levels. For the biomass, there is no perceptible differentiation of N levels within a crop. The accuracy of crop classification with reference to N levels is similar from both RF and SVM algorithms. However, RF algorithm offered substantially higher classification results when the N status is ignored. In contrast, the quality of biophysical modelling is very high and is similar from both the algorithms. Weather conditions and sub-field level environment-induced variations in the crop growth likely are

* Corresponding author. Fax: +91 471 2568462.

E-mail addresses: rao@iist.ac.in (R.R. Nidamanuri), rejivipin@gmail.com (R. Jayakumari), amramiya@gmail.com (A.M. Ramiya), astor.thom@gmail.com (T. Astor), mwach@uni-kassel.de (M. Wachendorf), buerkert@uni-kassel.de (A. Buerkert).

<https://doi.org/10.1016/j.biosystemseng.2022.08.005>

1537-5110/© 2022 IAgriE. Published by Elsevier Ltd. All rights reserved.

the factors responsible for the reduced sensitivity of remote sensing data to crop N levels at the patch level.

© 2022 IAgE. Published by Elsevier Ltd. All rights reserved.

1. Introduction

Monitoring crops during key phenological growth stages, and quantifying biophysical characteristics vis-à-vis nutrient status are vital for precision agriculture. Crop discrimination, and estimation of biophysical crop parameters at the plant or patch level help in precision site-specific agricultural crop management. Remote sensing has been widely used in crop monitoring at regional, national, and global levels. (Kolotii et al., 2015; Shelestov et al., 2015; Camacho, Cernicharo, Lacaze, Baret, & Weiss, 2013). Crop species-level discrimination and estimation of biophysical parameters have been very active areas of research in remote sensing (Astor, Dayananda, Nautiyal, & Wachendorf, 2020; Dayananda et al., 2019; Li et al., 2015). To mitigate the limitations in the availability of multi-temporal multispectral imagery, single date hyperspectral imagery has also been used to classify field crops (Neto, Lopes, Toledo, Zolnier, & Silva, 2018; Waldner, Canto, & Defourny, 2015; Nidamanuri & Zbell, 2011). Depending on the crop types and spatial resolution of the imagery used, 60–90% of accuracy has been reported.

The current suite of remote sensing satellites provides high-resolution data at spatial resolutions appropriate to identify crop type and estimate biophysical (e.g. biomass) parameters at the field scale. Most contemporary remote sensing satellites such as GeoEye-1, WorldView-III, and WorldView-IV offer multispectral data at a spatial resolution fine enough to capture within-field variations. However, despite high spatial and spectral resolutions, optical remote sensing data are limited in providing quantifiable features for crop discrimination and biophysical characterisation at sub-field scale with explicit reference to the crop nitrogen (N) status. In a practical scenario, the effects of differential N treatments are observable mainly by the difference in structural parameters during crop growth. The existence of inherent spectral similarities among crops and other vegetation types in the reflectance domain, even in hyperspectral data, has also been reported (Hennessy, Clarke, & Lewis, 2020; Nidamanuri & Zbell, 2013; Price, 1994). The delicate greenness and vigour sensitive spectral features with different N treatments at the ground or airborne level lose sensitivity at the satellite level. In contrast, the discernible features for crop discrimination and biophysical characterisation at different N levels are mainly related to the crop's structural–geometrical attributes.

There are two types of biophysical parameters relevant to crop phenotyping. The first category comprises directly measurable tangible primary plant parameters (e.g. height, crown area) and forms the primary determiners of crop physical and functional attributes. The second category is intangible and not directly measurable (e.g. yield, biomass, vigour) but are

frequently derived from the primary parameters. Both categories of parameters are required for functional descriptions of crops from a precision agriculture perspective. Plant height has a direct linear relationship with biomass for a range of standing crops (Poorter et al., 2012; Franco & Kelly, 1998). Plant crown area is a vital structural parameter that exhibits a linear relationship with growth and biomass accumulation across the phenological cycle. For many vegetable crops, plant height saturates at the ‘maturity’ phenological growth stage. Further vegetative development of the plant is reflected mainly in the lateral expansion of plant components characterised by crown area. Therefore, the response to a plant’s uptake of N is primarily evident in its lateral structural growth. The non-linear relationship between N levels and biomass can be modelled better with plant crown area. Therefore, remote sensing technologies for sub-field or patch level crop discriminations or biophysical characterisation are crucial for site-specific within-field level predictions of crop growth.

Optical remote sensing has severe limitations in providing tangible estimates of crop structural attributes such as height and crown area. Light Detection and Ranging (LiDAR) is a promising remote sensing technology for retrieving the precise vertical structure of crops. Complementary to the spectral features of multispectral imagery, LiDAR data, a point cloud, offers geometrical features for direct estimation of canopy structural parameters such as crop height, and canopy area at a finer spatial scale. Precise crop discrimination and biophysical characterisation can be achieved from the data level fusion of multispectral and LiDAR remote sensing data. This technique has been attempted for forest structure characterisation and orchard crops using airborne LiDAR point clouds (Manzanera et al., 2016; Liu & Bo, 2015). However, due to crop plants’ low height and complex background soil interactions, geometrical characterisation of crops requires very high-density LiDAR point cloud and scans from multiple facets. Terrestrial laser scanning (TLS) has emerged as one of the sophisticated technologies for the high-density LiDAR point cloud. Therefore, fusion data from TLS and high-resolution multispectral sensors is a viable strategy for high-resolution crop discrimination and biophysical characterisation of crops. The objective of this research, therefore, was the object-based discrimination and biophysical characterisation of three structurally different vegetable crops: cabbage (*Brassica oleracea* L.), eggplant (*Solanum melongena* L.), and tomato (*Solanum Lycopersicum* L.) at the patch level with explicit reference to crop N status by data fusion of TLS and very high-resolution multispectral imagery. The hypothesis tested was that the synergistic fusion of multispectral imagery and LiDAR point cloud allow nutrient specific vegetable crop discrimination and biophysical quantification at the plant or patch level.

2. Materials and methods

2.1. Study site and experimental design of crop growing plots

Using a factorial design, three different vegetable crops: cabbage, eggplant, and tomato, were grown on the experimental plots set up at the research farms of the University of Agricultural Sciences, GKVK Campus, Bengaluru, from February to June 2017 (Fig. 1). The experimental plots were irrigated through a drip irrigation system.

The crop growth set-up contained 12 plots of size $12\text{ m} \times 18\text{ m}$, each of which was subdivided into three subplots of $6\text{ m} \times 12\text{ m}$ with four replications, thus resulting in a total of 36 subplots. The sub-plots were randomly supplied with three different levels of mineral N fertiliser, designated as low, medium, and high. Following the agro-climatic zone based regional standards of fertilisation recommendations, the rate of N fertiliser for the different treatment levels was estimated based on rows. Accordingly, urea was applied for the 'medium N' at the rate of 46 kg N ha^{-1} for tomato, 60 kg N ha^{-1} for cabbage, and 50 kg N ha^{-1} for eggplant. Based on this, the 'high N' and 'low N' referred to 50% more and 50% less, respectively. Apart from the N fertiliser, a blanket application of phosphorus (P) and potassium (K) at the rate of 17.5 kg P ha^{-1} and $19.9, 41.5$, and 16.6 kg K ha^{-1} for tomato, cabbage, and eggplant was made at the time of sowing.

2.2. Data acquisitions

2.2.1. LiDAR point cloud acquisition

We used three different types of remote sensing data, two primary datasets and a derived dataset: LiDAR point cloud, high-resolution multispectral satellite imagery, and the dataset generated by fusion of these two remote sensing data types. LiDAR point clouds were acquired on 22 May 2017 using a high-density terrestrial laser scanner (TLS) (FARO 350^S, FARO Technologies Inc., USA) mounted on a height-adjustable tripod. The TLS used for point cloud acquisition is a single return topographic laser scanner operating at 1550 nm with a maximum target range of 350 m. Maintaining an optimal point posting distance of 6 mm, 15 scans were acquired from different locations in the study site. Several retro-reflecting target spheres were positioned across the plots for ensuring co-registration of the point clouds acquired from different scans. For geo-referencing and co-registration of the point clouds, geolocation coordinates at each scan position of the TLS and the reference target reflectors were recorded using a high accuracy differential global positioning system (DGPS) (Model: ICG70T; Make: Leica Geosystems, Switzerland).

2.2.2. High resolution satellite imagery

Multispectral satellite imagery was acquired on 22 May 2017 from the WorldView-III satellite in both multispectral and panchromatic modes. The spatial resolution of the imagery in multispectral and panchromatic mode is 1.2 m and 0.5 m,

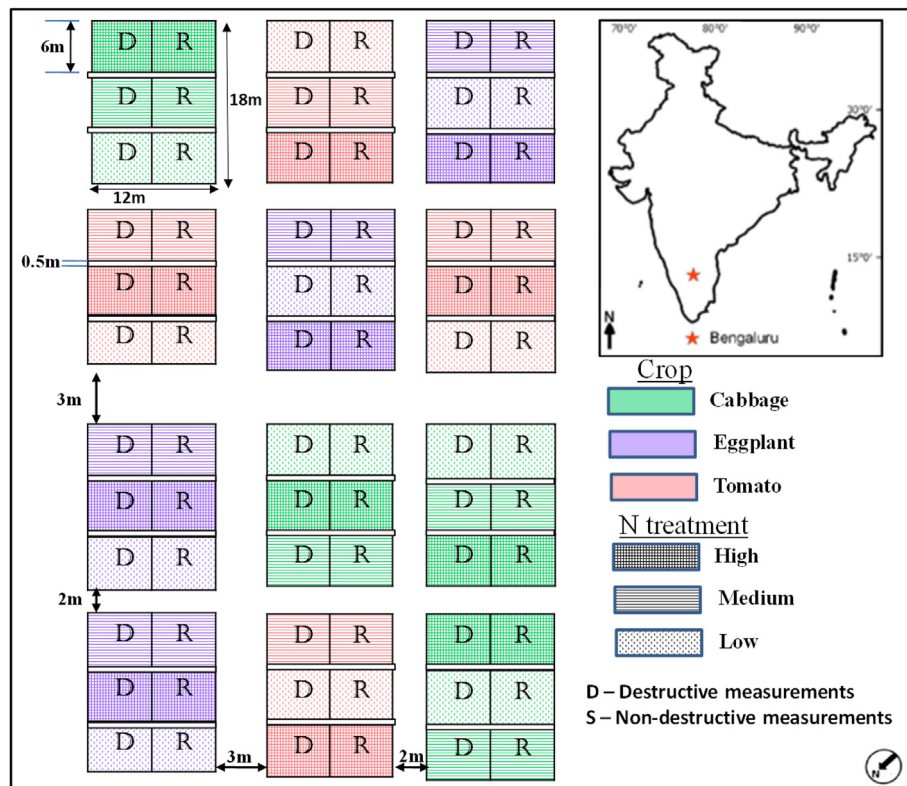


Fig. 1 – Location of the study site and layout of the experimental set-up designed for reference plots of the crop growing experiments at the experimental station of the University of Agricultural Sciences Bangalore (UASB), GKVK, Campus, India.

respectively. The multispectral imagery was acquired in eight spectral bands of the sensor covering the VNIR region of the electromagnetic spectrum (band 1 (coastal blue): 400–450 nm; band 2 (blue): 450–510 nm; band 3 (green): 510–580 nm; band 4 (yellow): 585–625 nm; band 5 (red): 630–690 nm; band 6 (red edge): 705–745 nm; band 7 (near IR1): 770–895 nm; band 8 (near IR2: 860–1040 nm)). The WorldView-III satellite acquires high resolution panchromatic imagery in the 450–800 nm region of the electromagnetic spectrum.

2.2.3. Ground truth biophysical measurements

We acquired ground truth measurements of crop type, height, crown area, and biomass of the three crops on each sampling date before collecting the LiDAR point cloud. The sub-plots were marked into two distinct regions, R and D, for undertaking, respectively, non-destructive and destructive sampling of plant measurements. Plant height was measured with a long meter scale to the nearest centimetre. In each subplot, the average height of 30 plants was calculated. The crown area was calculated by measuring distance measurements of plant crowns in the N–S and E–W directions. In each sub-plot, three individual plants were randomly harvested for computing

reference biomass measurements. The biomass measurements were up-scaled at the plot level and expressed as ton/hectare ($t\text{ ha}^{-1}$). The ground truth measurements were used in the calibration of discrimination models and for validation and accuracy assessment of the results.

2.3. Data processing

Data processing consisted of ground filtering, canopy height modelling and crop area segmentation, object-based classification, and biomass estimation as a function of different levels of N. The methodological process flow adopted in this work is shown in Fig. 2. The following subsection describes the various processes and techniques used in this work.

2.3.1. Pre-processing of datasets

For each sampling date, the multiple scans of raw LiDAR point clouds were co-registered using the pair-wise registration process proposed by Liu et al. (2017) with further modification for application in this work. The pair-wise registration procedure offers precise point cloud registration for most engineered surfaces and indoor environments. However, we

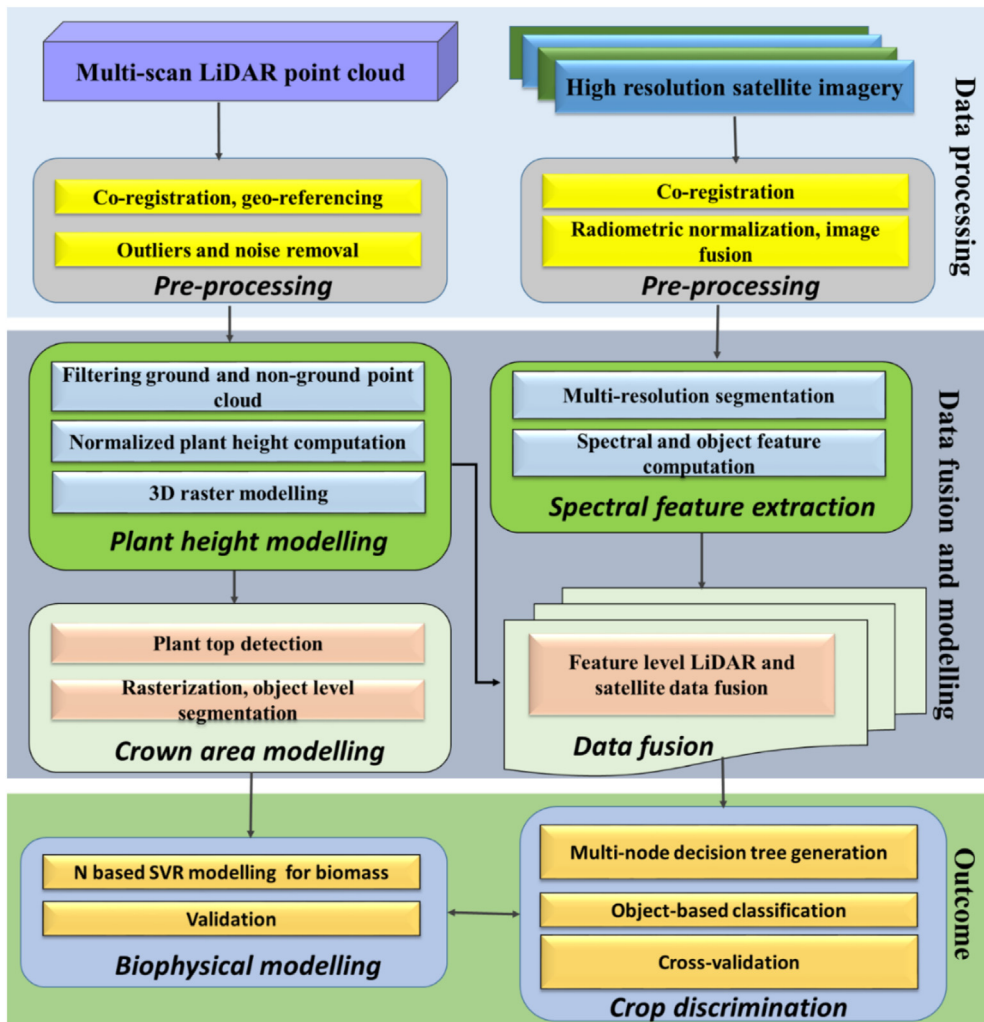


Fig. 2 – Methodological process flow indicating key steps from the datasets acquisition to the crop discrimination and biophysical characterisation of crops at the study site of University of Agricultural Sciences, Bengaluru, India.

observed local plant-environmental conditions: the soft nature of vegetable plant components and swift wind patterns caused the point cloud scans to lose the sturdy geometric corners. Therefore, the registration procedure was performed by establishing multi-scan correspondences based on the tie points generated using the manual-guided sphere fit algorithm. Outliers in the point cloud were removed by applying a local neighbourhood threshold algorithm based on a $3 \times 3 \times 3$ grid cell dimension.

The inherent radiometric and atmospheric distortions in the multispectral imagery were removed using a radiative transfer modelling based flexible atmospheric compensation technique (FACT) (Jha, Nidamanuri, Manohar, 2021). The spatial resolution of the multispectral imagery was enhanced to 0.5 m by fusion of the multispectral imagery with the panchromatic imagery using the Gram–Schmidt image fusion method (Mhangara, Mapurisa, & Mudau, 2020). Using the DGPS based coordinates as ground control points (GCP) in a polynomial approximation, the high-resolution imagery was co-registered (Yang et al., 2016) with the LiDAR point cloud to remove residual geometrical inconsistencies and pixel-point positional misalignments. Figure 3 illustrates example scans of LiDAR point cloud, the processed and co-registered point cloud and a false colour composite of the satellite imagery used.

2.3.2. Point cloud filtering and canopy height modelling

We acquired the LiDAR point cloud from multiple perspective positions at a finer surface sampling of 6 mm to allow crop plant level structural–biophysical characterizations. The proportion of laser returns of soil and other non-crop features in and around the experimental plots was higher than the

laser returns from the crop plant features. To minimize the computational challenges and enhance structural data representation, we filtered the LiDAR point cloud for generating point cloud of only crops using the progressive triangular irregular network (TIN) densification (PTD) method (Axelsson, 2000). The initial ground points were identified by searching for the lowest elevation points in each tile in the dataset that was divided into several tiles. A 2.5D reference surface was constructed, generating a triangular irregular network (TIN) considering the ground elevation points as the nodes. Based on the criteria of the point's distance to the TIN facet, the angle between the TIN facet and the threshold of the line connecting a point with the closest vertex of the facet, the unclassified points were added to the set of ground points. All classified ground points were appended to the TIN. All points in the point cloud were classified as belonging to ground or non-ground based on the progressive triangulation. The ground points were not considered for further analysis. The elevation of the point cloud pertaining to only crops was normalized to the surface level of the experimental plots, and the point cloud was rasterized to generate the digital crop plant level canopy height model (CHM).

2.3.3. Crown area modelling

Crown area is one of the primary patch level structural–biophysical parameters that provide crop-specific diagnostic information for discrimination and growth status estimation. Thanks to the high density of point cloud from TLS, it was possible to retrieve crown area for the crops considered. The computational approach adapted has two key stages: locating and identifying crown top and areal

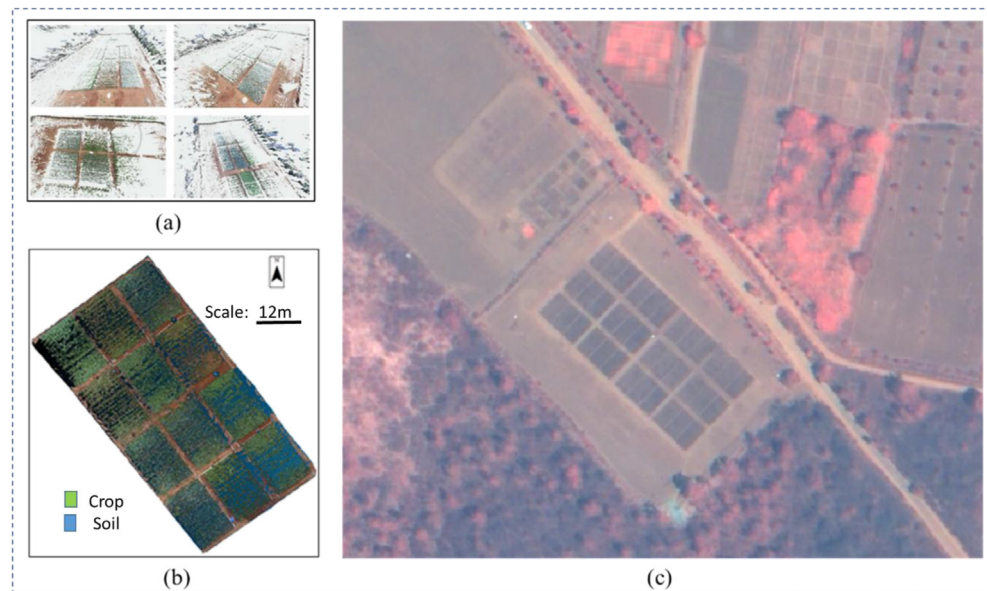


Fig. 3 – Visualization of the TLS point clouds and satellite imagery: (a) raw TLS scans acquired from four different scan positions, (b) processed LIDAR point cloud, and (c) a false composite (FCC) of the satellite imagery acquired (imagery spectral band assignment: red: near-infrared wavelength; green: red wavelength; blue: green wavelength) over the experimental station of the University of Agricultural Sciences Bangalore (UASB), GKVK, Campus, India. (For interpretation of the references to colour in this figure legend, the reader is referred to the Web version of this article.)

segregation and delineation of plant crowns. Corresponding to each height value in the CHM, plant crown tops were recognised using the variable window filtering (VWF) algorithm (Popescu & Wynne, 2004). This algorithm adaptively defines the local maxima for locating potential crown top within the window radius. The size of the window changes depending upon the height. The pixel with the maximum height value was approximated as the centre of the crown top. Finally, plant level crowns were delineated applying a marker-controlled watershed segmentation algorithm (Beucher & Meyer, 1993), substituting crown tops as centroids of the intensity distribution. The residual disconnected mass of point segments and segments without associated crown tops were eliminated from the resulting crown area model.

2.3.4. Crop discrimination

With explicit reference to different N levels, crops were discriminated by supervised classification of two datasets: very high-resolution WorldView-III imagery, and the LiDAR point cloud independently and the data generated from the fusion of these two datasets. Multi-modal data fusion can be achieved at various abstraction levels of data - pixel, feature, and decision. Compared to a raster imagery, LiDAR point cloud is unorganised and is spatially discrete. The unique geometrical features of LiDAR point cloud are best retained in the 3D perspective of the point cloud. We, therefore, adopted a feature fusion approach for fusing the LiDAR point cloud and multispectral imagery. Geographically meaningful object-based image classification is an apt technique for exploiting the rich spatial features of high-resolution remote sensing data (Blaschke, 2010) and enhancing data-interoperability compliance for operational use of remote sensing data-based products in agriculture. Since the spatial resolution of the datasets is very high (0.5 m for imagery and plant level for LiDAR point cloud), we opted for object-based image classification rather than the classical pixel-level classification. The object-based classification has two critical tasks – image segmentation and supervised classification.

Multi-resolution segmentation (MRS) (Baatz & Schäpe, 2000) is one of the widely used approaches at the operational level in many remote sensing applications (Nidamanuri & Zbell, 2011). The MRS algorithm, a region-based image segmentation technique, produces object-level image segments by user-dependent iterative optimisation of hyper-parameters – scale, shape, and compactness which control the spectral variance, heterogeneity, and boundary adherence. Image objects are created by grouping spatially contiguous pixels until reaching a threshold (scale parameter) representing the image object's upper level of spectral variance. To eliminate noise and for minimising the fractal borders, the image object's spectral variance at various levels of approximation was weighted with the image object's shape parameters. The quality of image segmentation varies substantially with the changing values of the user-dependent hyper-parameters. To ensure model convergence and avoid subjective segmentation, we applied a supervised method for hyper-parameter optimisation and selection suggested by Tong, Maxwell, Zhang, and Dey (2012). The test object boundaries required for evaluation were extracted from the ground truth map.

The LiDAR point cloud and multispectral imagery were fused by pairing up plant height and crown area with geographically corresponding image segments. This feature level fusion enables the computation of a range of crop plants' spatial, spectral, and geometrical features.

2.3.5. Supervised classification

Fusion of the LiDAR point cloud and multispectral imagery enables the generation of high dimensional feature space containing linear and non-linear variables of spectral and geometrical relevance. The effective volume of the feature space, spatial aggregation, and numerical range of features call for supervised classifiers with adaptive architectures. We applied two sophisticated used machine learning methods – Random Forest and Support Vector Machines (SVM) on the remote sensing datasets for supervised classification at two different levels of data aggregation: (i) at the sub-plot level with explicit reference to different N levels, and (ii) at the crop plot level without reference to the N level.

RF is a robust non-parametric supervised machine learning algorithms algorithm and builds decision trees on different training samples (Belgiu & Drăguț, 2016; Breiman, 2001). Due to its distinct feature of handling both continuous and categorical variables, the RF algorithm can be used for classification and regression tasks. SVM has been one of the widely used statistical machine learning algorithms with flexibility of adapting to different levels of dimensionality in the datasets (Razaque, Ben Haj Frej, Almi'ani, Alotaibi, & Alotaibi, 2021; Cortes & Vapnik, 1995). Similar to the RF, SVM can be used for classification or regression problems. In the RF algorithm, each decision tree is independently produced without any pruning, and each node is split using a user-defined number of features (M_{try}), selected at random. By growing the forest up to a user-defined number of trees (N_{tree}), the algorithm creates trees with high variance and low bias. Based on the heuristics, we chose the values of N_{tree} and M_{try} as 650 and 3, respectively. About two-thirds of the samples (referred to as in-bag samples) were used to train the model, with the remaining one third (referred to as out-of-the bag samples) used for cross-validation for estimating the quality of the model's performance. The final classification decision is taken by averaging (using the arithmetic mean) the class assignment probabilities calculated by all produced trees. The unlabelled data input is thus evaluated against all decision trees created in the ensemble, and each tree votes for class membership. The membership class with the maximum votes will be the one that is finally selected. The SVM algorithm was implemented for supervised classification using the LIBSVM library developed by Chang and Lin (2011). The values for loss function ϵ , error penalty factor C, and kernel function were estimated based on iterations and heuristics as suggested by Meyer, Reudenbach, Hengl, Katurji, and Nauss (2018). The kernel used is the radial basis function (RBF).

Considering that, in many cases, crops are classified without reference to the nutrient status, we assessed the potential of LiDAR point cloud and multispectral imagery at two levels of data representation – the fine and the coarse level. At the fine level, the classification was done at the individual sub-plots with explicit reference to the different nutrient treatments of the crops. Therefore, the purpose of the

classification was to know whether the LiDAR point cloud or multispectral imagery offers crop discrimination maintaining the sensitivity to different N levels of crops. At the coarse level, the purpose of classification was mainly to obtain the benchmark crop discrimination results from LiDAR point cloud or multispectral imagery without reference to the N status of the different vegetable crops considered. The results of the classification were validated by 5-fold cross-validation.

2.3.6. Biophysical characterization

2.3.6.1. Crown area estimation using multispectral imagery. Estimating tree crown area using high-resolution remote sensing data has been well documented under individual tree crown detection (ITDC) (Otsu, Pla, Duane, Cardil, & Brotons, 2019; Wang, Gong, & Biging, 2004). Considering the specific context of the surface objects (i.e. relatively small vegetable crops), we have extended the application of the “valley following” method of image segmentation and ITDC for crown area estimation for the crops considered. To match the location-sensitive spatial resolution and comparison with the LiDAR point cloud-based estimates, we resampled the multispectral imagery to 10 cm resolution and applied a super-pixel based spatially continuous clustering algorithm for the initial candidate plant objects generation. The possibility of within-canopy gaps induced soil pixels in the plant-context image object was reduced by histogram thresholding of the spectral indices. The boundaries of plant-location sensitive crowns generated were filtered for spatial continuity and connectivity using morphological operators.

2.3.6.2. Biomass estimation using multispectral imagery. Similar to the scheme implemented for crop discrimination, biomass was estimated using multispectral imagery and LiDAR point cloud independently and with the fused dataset. The spectral attributes sensitive to the crop structural and biophysical features are indirect and relative to differential spectral features. They are mainly embedded in the differential reflectance features in various spectral bands across the optical range of the electromagnetic spectrum. Different spectral indices highlight the nature of the crop's response in the recorded spectral radiance in the multispectral imagery. Therefore, we used various spectral indices as surrogate variables for biomass modelling using the multispectral imagery (Kross, McNairn, Lapen, Sunohara, & Champagne, 2015; Fu, Yang, Wang, Song, & Feng, 2014). Based on the sensitivity to the vegetation structure, seven standardized and derived spectral indices, namely, the Enhanced Vegetation Index (EVI), Soil-Adjusted Vegetation Index (SAVI), Normalized Difference Vegetation Index (NDVI), Normalized Difference Water Index (NDWI), Green Normalized Difference Vegetation Index (GNDVI), Blue Normalized Difference Vegetation Index (BNDVI), and Wide Dynamic Range Vegetation Index (WDRVI) were computed from the multispectral imagery (Guan, Abd-Elrahman, Fan, Whitaker, & Wilkinson, 2020; Chao, Liu, Zhang, Ying, & Song, 2019; Kayad, Sozzi, Gatto, Marinello, & Pirotti, 2019; Chlingaryan, Sukkarieh, & Whelan, 2018; Wang et al., 2017; Ramoelo et al., 2015; Adam, Mutanga, Abdel-Rahman, & Ismail, 2014). A detailed mathematical

formulation of these spectral indices is available in Thenkabail, Lyon, and Huete (2018). Given the availability of reference biomass measurements, the crop biomass was estimated using the SVM and RF as regression modelling algorithms, considering the spectral indices as predictor variables.

The high-density capability of the TLS used in this work enabled acquiring LIDAR point cloud retaining the individual plant structures in the data. However, the size of vegetable crop plants, expressed by canopy extent and height, was smaller than the spatial resolution of most high-resolution multispectral sensors, including the Worldview-III data. Thus, distinct retention of crop plant structure was not functionally possible, per se. Most remote sensing studies attempting to retrieve canopy area and height are directed at natural vegetation such as a forest. In contrast, the LiDAR point cloud enables retrieval of canopy area and height as direct variables. Hence, we retrieved only the biomass from the multispectral imagery for further comparison with the estimations from the LiDAR point cloud.

2.3.6.3. Biomass estimation using LiDAR point cloud and the fused dataset. To account for the linear and non-linear patterns of plant height and crown area, we applied the same machine learning algorithms used for classification RF and SVM in the regression mode, Support Vector Regression (SVR; Shim & Chang, 2011) for modelling the crop biomass for various levels of N. The values for the hyper-parameters of the SVR algorithm (loss function ϵ , error penalty factor C, and kernel function) were estimated based on heuristics and cross-validation. Adapting a similar methodological framework used for estimating biomass from the LiDAR point cloud, the fused dataset, which contained spectral attributes appended to each discrete point in the point cloud, was used for biomass estimating through the SVM and RF algorithms. As the dimensionality of the feature space was higher for the fused dataset, the divergent set of features were optimized by an iterative forward feature selection method (Meyer et al., 2018) to choose the most influential variables.

2.3.7. Validation

Biophysical parameters: Using the reference biophysical measurements, the quality of the predictions of biophysical parameters was assessed using the ‘Symmetric mean absolute percentage error (SMAPE)’ (Goodwin & Lawton, 1999) expressed as

$$\text{SMAPE} = \frac{100\%}{n} \sum_{i=1}^n \frac{|y_i - x_i|}{|y_i| + |x_i|} \quad (1)$$

where y_i is the estimated parameter, x_i is the measured parameter for a measurement pair i.

As indicators of the inherent variability in the reference data thereby benchmarking the variations in the biophysical modelling, the mean and standard deviations of the reference biophysical measured were also computed.

To understand the relevance of inherent variability in the field conditions, the mean and standard deviation of the measured biomass values plotted for different N levels.

3. Results

3.1. Crops discrimination with explicit reference to the nitrogen status

The results of the fine level classification from both classification methods depicting the discrimination of the vegetable crops with by to nutrient level are shown in Figs. 4 and 5 as well as the corresponding statistical measures of accuracy, and confusion matrix, obtained from the cross-validation in Figs. 6 and 7. Evident from the accuracy metrics and the spatial diffusion of the segments of two different crops, the quality of crop discrimination from the multispectral

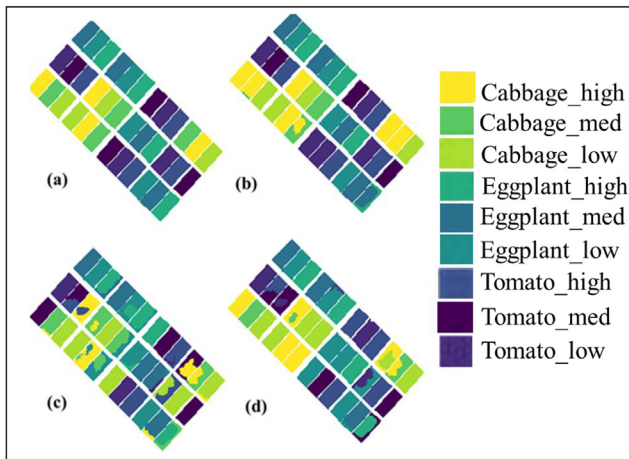


Fig. 4 – Classification results from the RF algorithm with reference to N treatment obtained from (a) ground truth, (b) from the fused dataset generated from multispectral imagery and LiDAR point cloud, (c) from LiDAR point cloud, and (d) from multispectral imagery of our field study site.

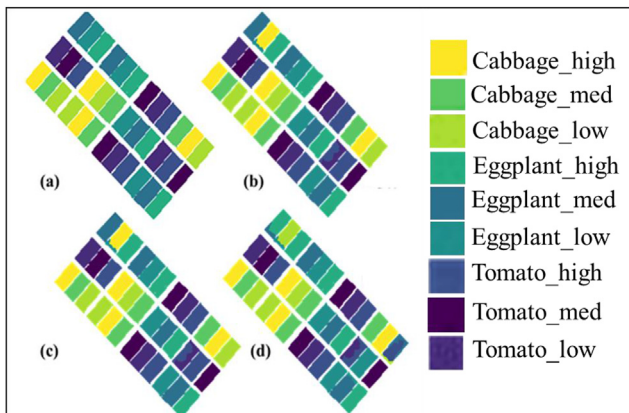


Fig. 5 – Classification results from the SVM algorithm with reference to N treatment; (a) ground truth, (b) from the fused dataset generated from multispectral imagery and LiDAR point cloud, (c) from LiDAR point cloud, and (d) from multispectral imagery of our field study site.

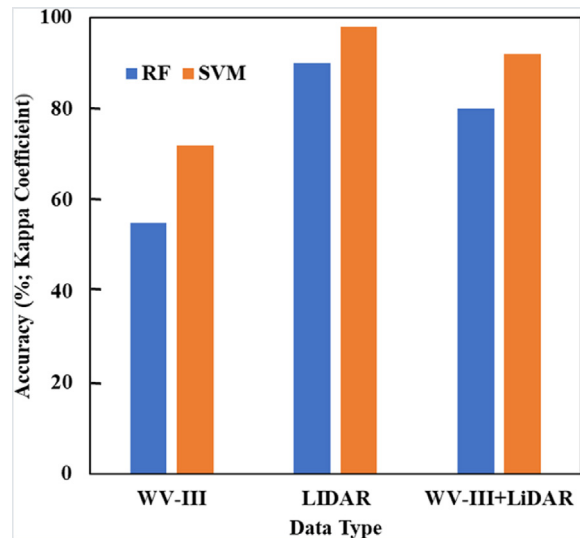


Fig. 6 – Overall accuracy (Kappa coefficient in percentage) of classification with reference to N level from RF and SVM algorithms; multispectral imagery (WV-III), LiDAR point cloud (LiDAR) and the fused dataset (WV-III + LiDAR) of our field study site.

imagery is poor. Multiple inter-crop confusion cases led to misclassification of a crop sub-plot (e.g. cabbage) wrongly labelling as another crop (e.g. tomato) and lowest accuracy (kappa accuracy of 56%). Compared to the results from multispectral imagery, the results from the LiDAR point cloud are somewhat better (overall accuracy of 79%), indicating a 23% higher accuracy, than the multispectral imagery results. This improvement can be ascribed to the apparent reduction in the mislabelling of the whole sub-plot to partial sub-plot, indicating the dominance of structural features in the discrimination. The classification results from the fused datasets are distinct (92% accuracy) and significantly better than the results from the individual sensors, supporting the hypothesis that spectral and structural features are vital for discriminating different crops by nutrient level. However, a few sub-plots are wrongly labelled by nutrient level, even though classification was correct for the crop type. For example, a sub-plot of cabbage with medium N was classified as a sub-plot of cabbage with low N. For the multispectral imagery, there is a substantial difference (about 20%) in the classification accuracy between the RF and SVM algorithms even though the difference is marginal with similar levels of accuracy for the LiDAR and fused datasets. Across datasets, the SVM algorithm offered relatively better classification results.

3.2. Crops discrimination without reference to the nitrogen status

The results of the classifications of the crops without specifying the N status are presented in Figs. 8 and 9. The estimated overall accuracy represented by kappa coefficient is plotted in Fig. 10. As evident from Figs. 9 and 10, the quality of crop discrimination with the multispectral imagery is reasonably

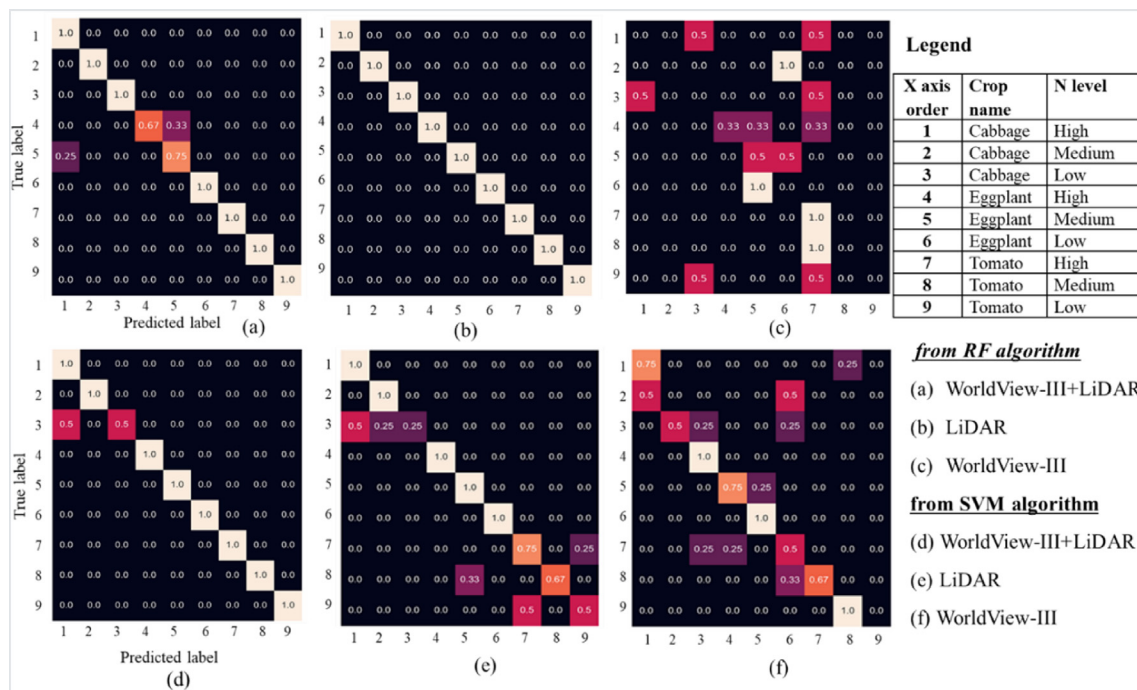


Fig. 7 – Confusion matrix generated from the validation of the results of crop classification with sensitive to N level from the fused dataset generated from multispectral imagery and LiDAR point cloud, from LiDAR point cloud, and from multispectral imagery using RF (a – c) and SVM (d – f) algorithms.

good, with an overall accuracy of about 80%. The performance gap of about 30% observed between the multispectral imagery and the LiDAR point cloud for different N levels has reduced to 7%. Indicating the continuance of the dominance of structural features, compared to the results from multispectral imagery, the classification results from using only the LiDAR point cloud are better, even though the margin of accuracy

difference was reduced to only 7%. In both cases, a few patches of cabbage were erroneously classified as tomato or eggplant. The crops are discriminated in the fused dataset with close to 98% accuracy. However, the margin of accuracy improvement is only 6%, indicating that either of the spectral or geometrical features alone can differentiate the crops without reference to the crops' N status. In contrast to the relatively similar performance of the RF and SVM algorithms for the classification according to the N level, there is a

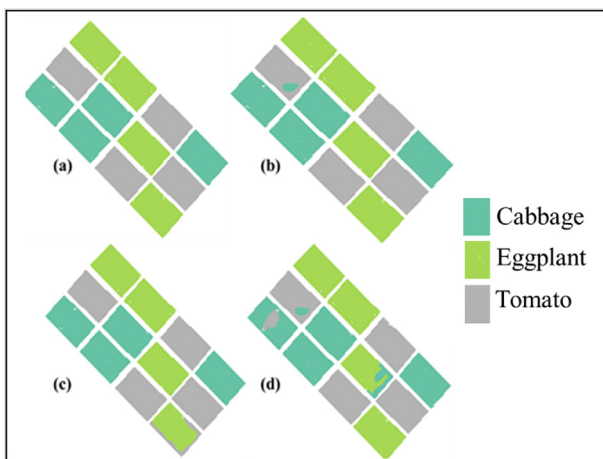


Fig. 8 – Classification results of RF algorithm without reference to N treatment obtained from (a) ground truth, (b) from the fused dataset generated from multispectral imagery and LiDAR point cloud, (c) from LiDAR point cloud, and (d) from multispectral imagery of three different vegetables at the experimental station of the University of Agricultural Sciences Bangalore (UASB), GKVK, Campus, India.

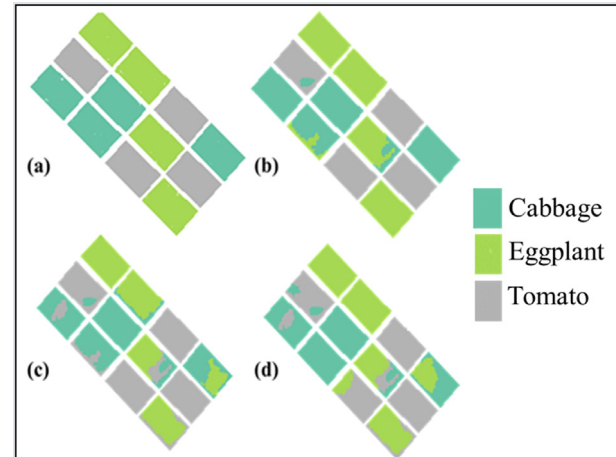


Fig. 9 – Classification results of SVM algorithm without reference to N treatment obtained from (a) ground truth, (b) from the fused dataset generated from multispectral imagery and LiDAR point cloud, (c) from LiDAR point cloud, and (d) from multispectral imagery.

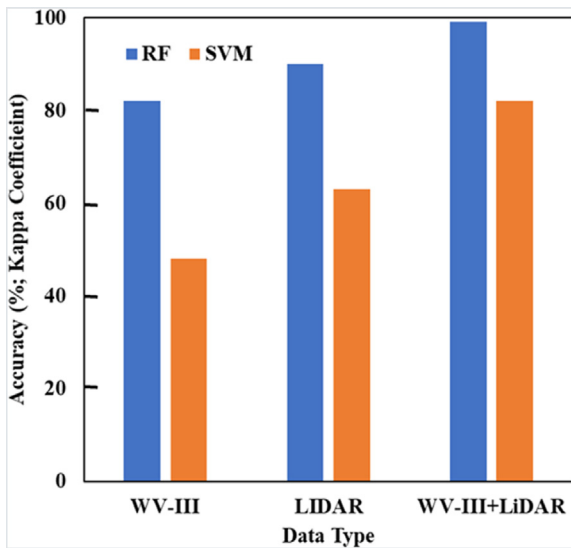


Fig. 10 – Overall accuracy (Kappa coefficient in percentage) of classification without reference to N level from RF and SVM algorithms; multispectral imagery (WV-III), LiDAR point cloud (LiDAR) and the fused dataset (WV-III + LiDAR).

substantial difference in the accuracy between them across the datasets when there is no reference to N level. As seen from Fig. 10, the accuracy of classification from the SVM algorithm is poor.

3.3. Estimation of biophysical parameters

Results of the crown area and biomass estimations using the LiDAR point cloud, multispectral imagery and the fused dataset using the RF and SVM algorithms in regression mode are presented in Figs. 11–18 and Tables 1–4. As evident from Table 1 and Figs. 11 and 12, the crown area estimates using the LiDAR point cloud exhibit a high degree of precision and accuracy across the different N treatments and the crops considered. Summarizing the influence of the regression modelling algorithm on the estimates, values of the coefficient of determination are presented in Table 2. Except for the marginal differences for the high N level, the performance of estimation is similar from both SVM and RF algorithms indicating the consistence of modelling (Figs. 11 and 12 and Table 2). The crown area varies linearly maintaining a stable one-to-one correlation with the measured values. The maximum error of estimation indicated by the SMAPE is about 15%. The range of the crown area of cabbage is relatively lower, and the full range variation is not apparent, though statistically exhibiting a linear trend.

Closely following the relationship observed with the crown area, the biomass estimated from LiDAR point cloud exhibits a consistently high correlation with the measured values. Compared to the plant crown area, the error of estimation quantified by SMAPE is marginally lower. However, the variation of the biomass as a function of N treatment exhibits an overlapping pattern suggesting the potential diffusion of biomass estimations across N treatments and crops (see Table 2, and Figs. 13 and 14).

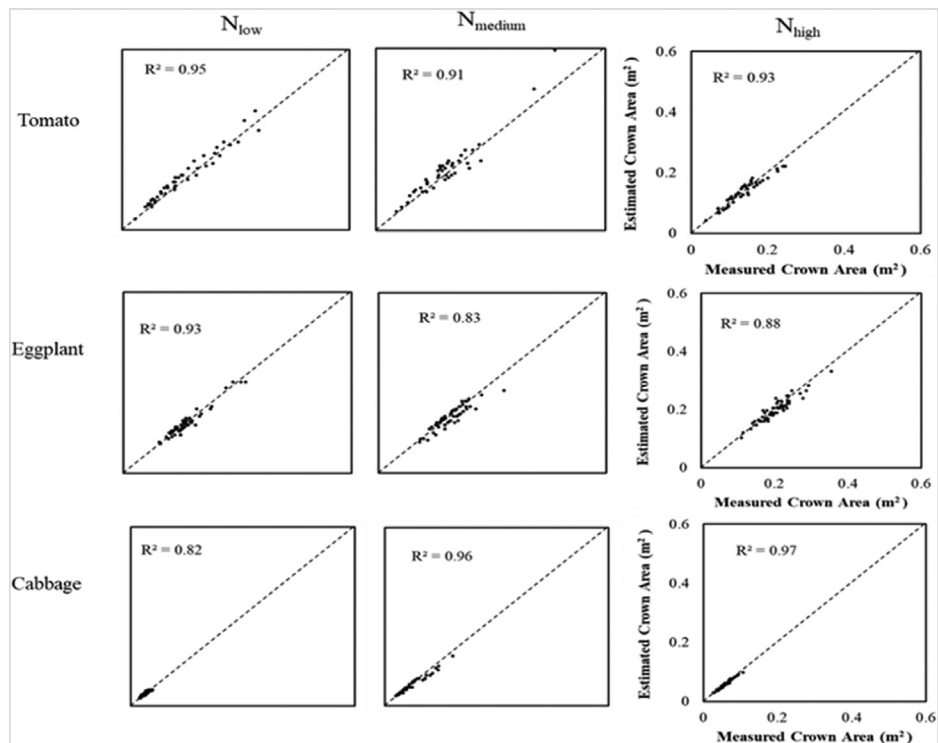


Fig. 11 – Comparison of the plant crown area estimated from LiDAR point cloud using the SVM algorithm with the reference measurements of three different vegetables at the experimental station of the University of Agricultural Sciences Bangalore (UASB), GKVK, Campus, India.

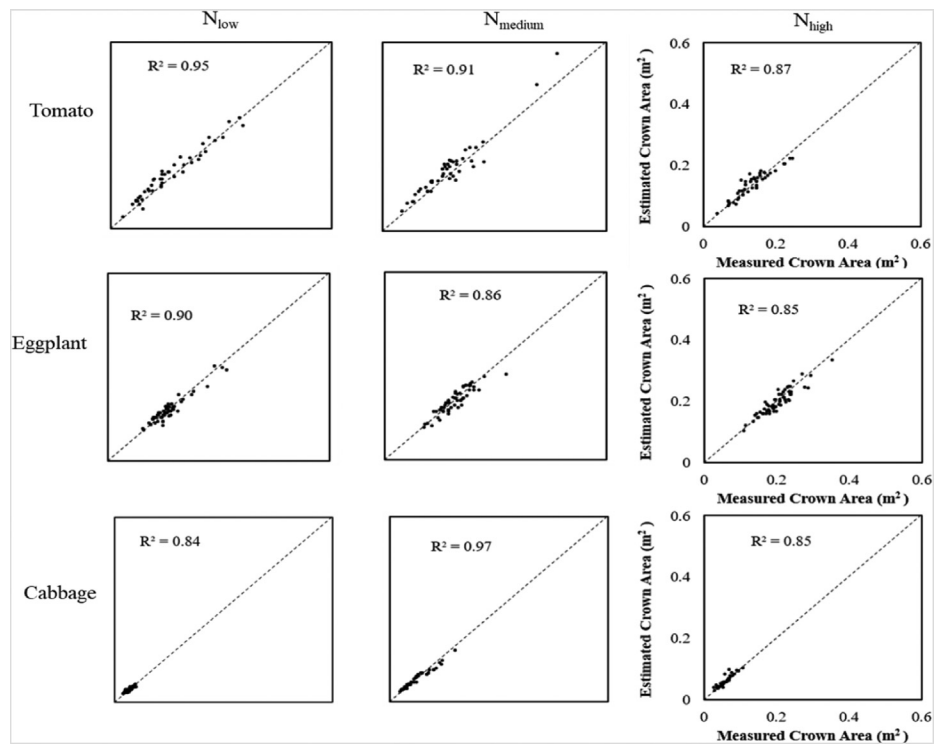


Fig. 12 – Comparison of the plant crown area estimated from LiDAR point cloud using the RF algorithm with the reference measurements of three different vegetables at the experimental station of the University of Agricultural Sciences Bangalore (UASB), GKVK, Campus, India.

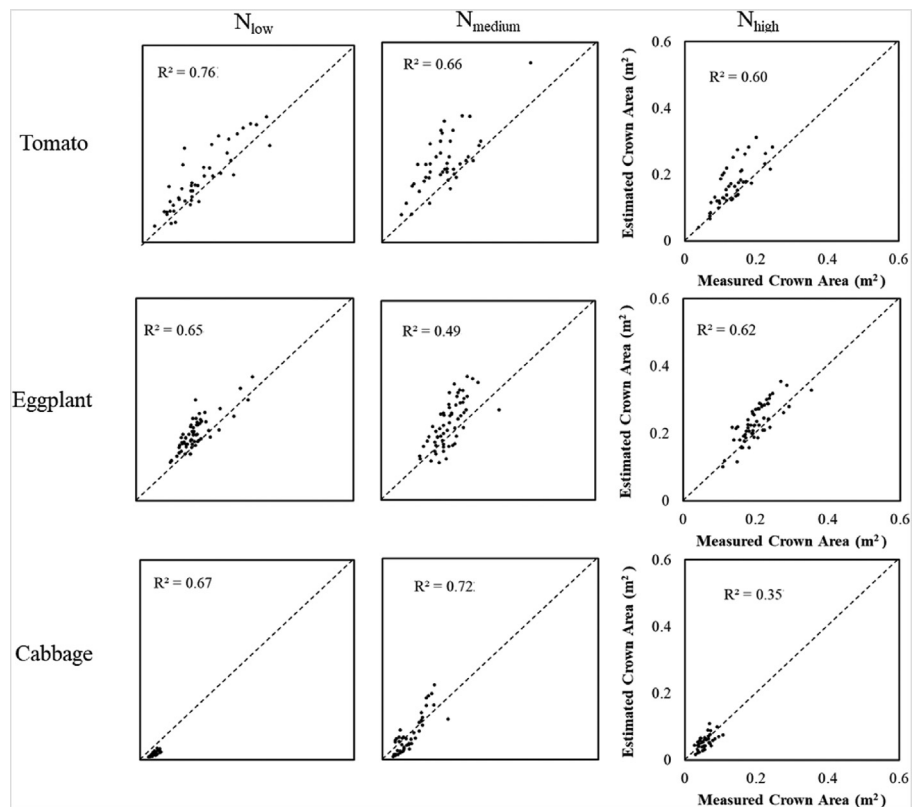


Fig. 13 – Correlation of the plant crown estimates obtained from multispectral imagery using SVM algorithm with the reference measurements of three different vegetables at the experimental station of the University of Agricultural Sciences Bangalore (UASB), GKVK, Campus, India.

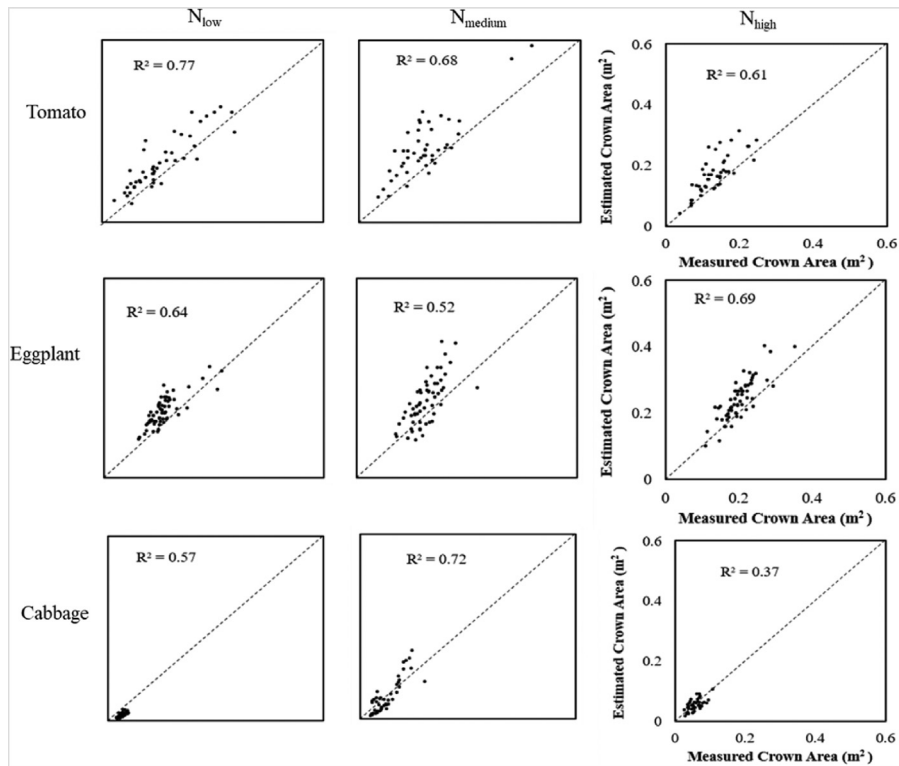


Fig. 14 – Correlation of the plant crown estimates obtained from multispectral imagery using the RF algorithm with the reference measurements of three different vegetables at the experimental station of the University of Agricultural Sciences Bangalore (UASB), GKVK, Campus, India.

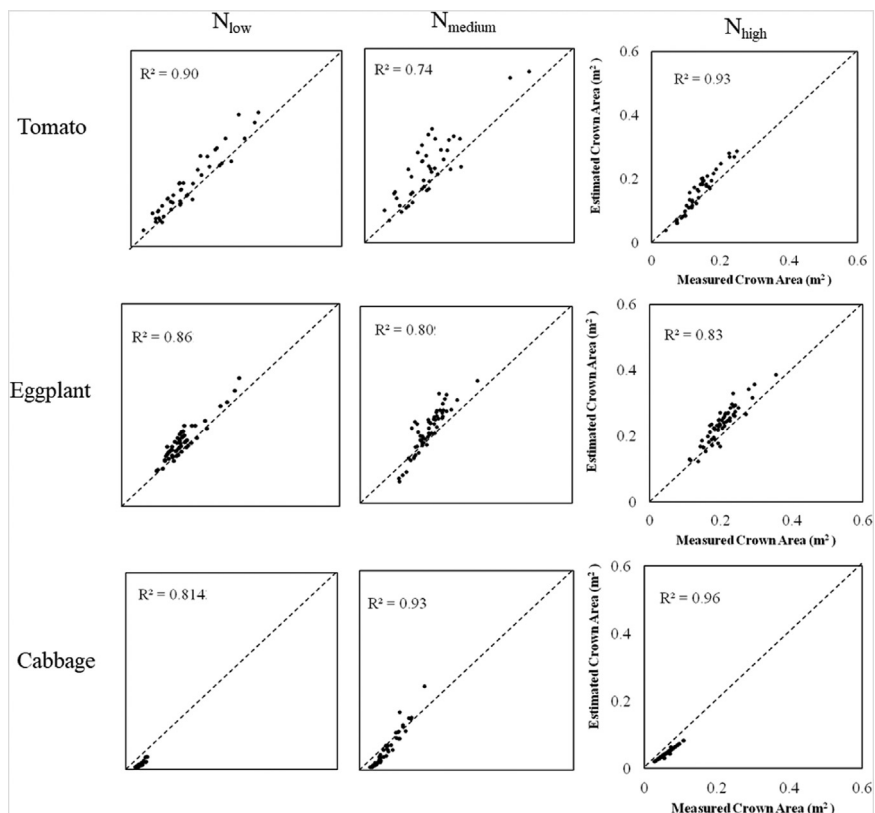


Fig. 15 – Comparison of the plant crown estimates obtained from the fusion of multispectral imagery (WorldView-III) and LiDAR point cloud using the SVM algorithm with the reference measurements of three different vegetables at the experimental station of the University of Agricultural Sciences Bangalore (UASB), GKVK, Campus, India.

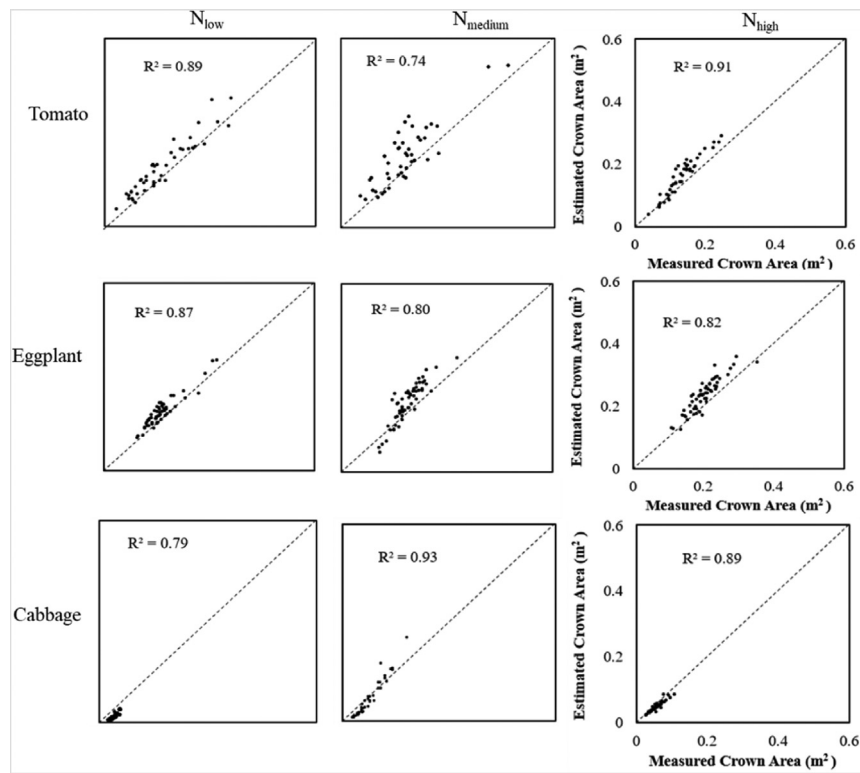


Fig. 16 – Comparison of the plant crown estimates obtained from the fusion of multispectral imagery (WorldView-III) and LiDAR point cloud using the RF algorithm with the reference measurements of three different vegetables at the experimental station of the University of Agricultural Sciences Bangalore (UASB), GKVK, Campus, India.

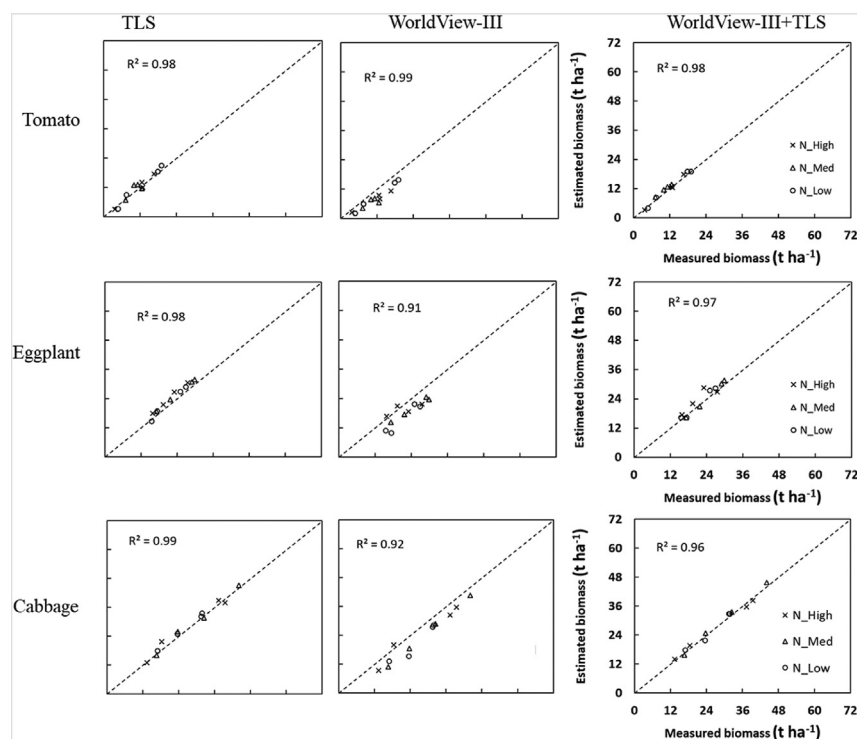


Fig. 17 – Comparison of the biomass estimates obtained from LiDAR point cloud (TLS), multispectral imagery (WorldView-III) and combination dataset generated by fusion of multispectral imagery and LiDAR point cloud using the SVM algorithm with the reference measurements of three different vegetables at the experimental station of the University of Agricultural Sciences Bangalore (UASB), GKVK, Campus, India.

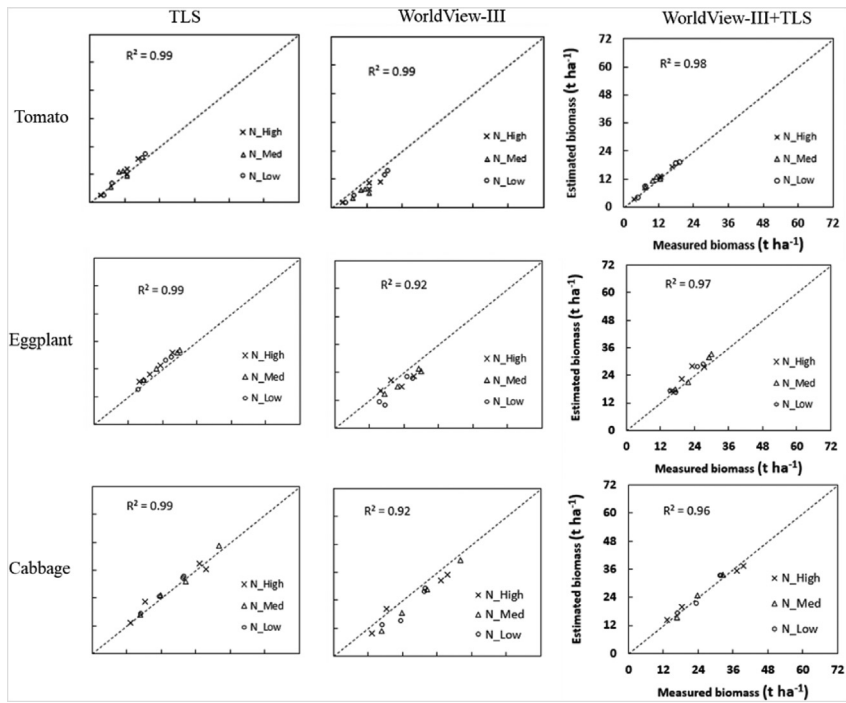


Fig. 18 – Comparison of the biomass estimates obtained from LiDAR point cloud (TLS), multispectral imagery (WorldView-III) and combination dataset generated by fusion of multispectral imagery and LiDAR point cloud using the RF algorithm with the reference measurements of three different vegetables at the experimental station of the University of Agricultural Sciences Bangalore (UASB), GKVK, Campus, India.

Table 1 – Estimates of overall accuracy and error (SMAPE) of plant crown area for different N treatments of a vegetable crop growing experiment at the University of Agricultural Sciences Bangalore (UASB) from the remote sensing datasets considered. The reference measurements of crown area are also included for ready reference. Values in blue colour correspond to the estimates from the RF algorithm and negative sign indicates underestimation.

Crop	Measured Crown Area (m ²)	Estimated Crown Area (m ²)	Remote sensing data type								
			TLS			WorldView-III			WorldView-III + TLS		
			Mean	Accuracy (%)	SMAPE (%)	Mean	Accuracy (%)	SMAPE (%)	Mean	Accuracy (%)	SMAPE (%)
Tomato	L 0.163	0.175	88.32	11.68	0.191	72.74	27.26	0.188	80.02	19.98	
		0.173	87.37	12.63	0.186	70.44	29.56	0.175	75.75	24.25	
		0.194	84.17	15.83	0.248	63.78	36.22	0.226	70.11	29.89	
	M 0.179	0.192	83.13	16.87	0.231	64.59	35.41	0.221	69.31	30.69	
		0.132	90.35	-9.65	0.166	69.31	30.69	0.154	80.36	19.64	
		0.129	88.37	-11.63	0.158	71.06	28.94	0.51	79.42	20.58	
Eggplant	L 0.169	0.167	92.85	-7.15	0.204	77.69	22.31	0.195	83.48	16.52	
		0.159	91.08	-8.92	0.193	79.64	20.36	0.194	84.11	15.89	
		0.191	90.36	-9.64	0.242	72.67	27.33	0.228	81.99	18.01	
	M 0.198	0.193	90.79	-9.21	0.231	74.31	25.69	0.217	83.75	16.25	
		0.205	92.4	-7.6	0.245	81.05	18.95	0.248	82.32	17.68	
		0.208	92.69	-7.31	0.241	82.79	17.21	0.232	84.59	15.41	
Cabbage	L 0.039	0.04	90.25	9.75	0.016	42.9	-57.1	0.016	67.44	-32.56	
		0.36	89.79	10.21	0.014	39.79	-60.21	0.018	68.75	-31.25	
		0.07	85.95	-14.05	0.038	56.23	-43.77	0.06	71.15	-28.85	
	M 0.076	0.068	84.31	-15.69	0.039	55.75	-44.25	0.063	71.79	-28.21	
		0.054	92.28	-7.72	0.043	67.47	-32.53	0.044	75.01	-24.99	
		0.061	92.69	7.31	0.046	71.59	-28.41	0.046	76.46	-23.54	

Table 2 – Coefficient of determination (R^2) summarizing the relative performance the regression modelling algorithms (RF and SVM) for estimating the crown area from different datasets.

	N_{low}		N_{med}		N_{high}	
Tomato						
Method	SVR	RF	SVR	RF	SVR	RF
TLS	0.95	0.95	0.91	0.91	0.93	0.87
WV-III	0.76	0.77	0.66	0.68	0.60	0.61
TLS + WV-III	0.90	0.89	0.74	0.74	0.93	0.91
Eggplant						
TLS	0.93	0.90	0.83	0.86	0.88	0.85
WV-III	0.65	0.64	0.49	0.52	0.62	0.69
TLS + WV-III	0.86	0.87	0.80	0.80	0.83	0.82
Cabbage						
TLS	0.82	0.84	0.96	0.97	0.97	0.85
WV-III	0.67	0.57	0.72	0.72	0.35	0.37
TLS + WV-III	0.81	0.79	0.93	0.93	0.96	0.89

Compared to the results obtained with the LiDAR point cloud, the estimates of biophysical parameters from multispectral imagery show a contrasting pattern (see Figs. 15 and 16 and Table 2). On the one hand, the crown area estimations exhibit a moderate to lower correlation with the measured crown area. The ‘low’ N treatment exhibits a relatively higher correlation with the measured values across the three crops. The quality of plant crown area estimations for the high N treatment was relatively poor. The lowest and highest error of the estimate is about 22% and 57%, respectively. On the other

hand, the estimates of biomass using multispectral imagery show a consistently higher correlation with the measured biomass (Figs. 13 and 14). They are comparable with the estimations from the LiDAR point cloud. However, this apparent strong correlation degrades to moderate levels of biomass estimations. The lowest and highest error of estimates is about 22% and 30%, respectively. The error reflected primarily the overestimation across the N treatments and crops (Table 2). Continuing the trend observed with the LiDAR point cloud, the results from RF and SVM algorithms match closely indicating consistency in the biomass estimations. If the reference to the N treatment condition was relaxed, the estimation of biomass using the multispectral imagery exhibits substantially better results (Table 3), especially for eggplant and cabbage.

The plant crown area and biomass estimates obtained from the fused dataset exhibit a systematically higher level of correlation and accuracy (Figs. 17 and 18, and Tables 1–4). Compared to the apparent contrasting behaviour of the overestimation of plant crown area and underestimation of the biomass from the multispectral imagery, the results from the fused dataset exhibit a consistent one-to-one trend across crops and N treatments. The variation of the estimates from the fused dataset for the plant crown area and biomass was very similar to the variation of the estimates from the LiDAR point cloud. Continuing the pattern observed with the LiDAR point cloud or multispectral imagery, the biomass estimates from the fused dataset also show considerable overlaps in the estimates for different N treatments (Figs. 13 and 14). Overall, the

Table 3 – Summary statistics of overall accuracy, prediction error (SMAPE) of the biomass estimated for different N treatments of a vegetable crop growing experiment at the University of Agricultural Sciences Bangalore (UASB) from the remote sensing datasets considered. For ready reference, measured biomass values are also presented. Negative values of SMAPE indicate the error of underestimation. Values in blue colour correspond to the estimates from the RF algorithm.

Crop	Measured Biomass (t ha ⁻¹)		Estimated biomass (t ha ⁻¹)	Remote sensing data type							
				TLS			WorldView-III			WorldView-III + TLS	
	Mean	Accuracy (%)		Mean	Accuracy (%)	SMAPE (%)	Mean	Accuracy (%)	SMAPE (%)	Mean	Accuracy (%)
Tomato	L	12.35	12.9 13.3 12.55	9.6	77.75	-22.25	12.57	98.21	1.79		
	M	11.85		8.22	69.38	-30.62	13.1	90.42	9.58		
	H	11.52		7.76	67.39	-32.61	11.62	99.1	0.9		
	L	21.26	10.98 22.25 23.14	10.98	98.31	-1.69	7.23	63.75	-36.25	11.02	98.74
	M	24.44		15.81	74.35	-25.65	22.13	96.08	3.92		
	H	21.46		16.25	75.44	-24.56	22.57	96.65	3.35		
Eggplant	L	25.97	26.25 25.69 23.65	26.25	93.12	6.88	19.98	81.72	-18.28	24.78	98.63
	M	29.22		20.14	81.53	-18.47	25.12	98.19	1.81		
	H	27.19		10.93	19.48	90.73	-9.27	23.75	90.38	9.62	
	L	25.97	27.12 26.84 29.63	90.13	9.87	20.17	91.26	-8.74	24.12	89.75	10.25
	M	29.22		21.05	81.05	-18.95	26.28	98.84	1.16		
	H	27.19		22.15	83.02	-16.98	26.85	97.69	2.31		
Cabbage	L	25.97	31.25 27.83	24.73	84.6	-15.4	29.93	97.66	2.34		
	M	29.22		25.41	85.79	-14.21	31.02	97.02	2.98		
	H	27.19	23.87 26.54	24.4	89.75	-10.25	26.9	98.95	-1.05		
				23.87	87.46	-12.54	26.12	96.75	-3.25		

Table 4 – Summary of the biomass estimation with no specific reference to N treatment. The estimated biomass is compared against the mean of the measured biomass. The SMAPE value in the negative sign indicates the error of underestimation. Values in blue colour correspond to the estimates from the RF algorithm.

Crop	Measured biomass ($t \text{ ha}^{-1}$)	Estimated biomass ($t \text{ ha}^{-1}$)	Remote sensing data source								
			TLS			WorldView-III			WorldView-III + TLS		
			Mean	Accuracy (%)	SMAP E (%)	Mean	Accuracy (%)	SMAP E (%)	Mean	Accuracy (%)	SMAP E (%)
Tomato	11.4	11.85 10.21	11.85	96.05	3.95	7.99	70.09	-29.91	11.94	95.26	4.74
			24.2	91.92	8.08	18.42	82.27	-17.73	23.55	94.82	5.18
			23.14	92.32	7.68	16.78	80.64	-19.36	21.65	95.35	-4.65
Eggplant	22.39	28.19 26.27	28.19	97.12	2.88	23.39	85.36	-14.64	27.7	98.91	1.09
			26.27	96.85	-3.15	21.84	83.46	-16.54	26.15	97.69	-2.31

estimation of plant crown and biomass from the fused dataset exhibits marginal to substantial improvements compared to the estimates from the LiDAR point cloud. As evident from [Tables 2 and 3](#), the estimates of crown area and biomass from RF and SVM algorithm vary only marginally, exhibiting both overestimation and underestimation without a systemic pattern.

To understand the relevance of inherent variability in the field conditions, the mean and standard deviation of the measured biomass values are plotted for different N levels ([Fig. 19](#)). The measured biomass exhibits substantial variations across N treatments and crops ([Fig. 19](#)). The intra-crop biomass variation was higher than the inter-crop biomass variation, thereby blurring the predictive boundaries of the non-parametric discrimination models used for fusion and estimation of biomass.

4. Discussion

High-resolution remote sensing has been extensively used to map and monitor crops from regional to national scales. In most studies, the typical mapping unit comprises a field of several hectares. This scale is appropriate for deriving overall estimates such as crop area, type and potential yield, and general crop health in landscapes where average field size is of several hectares. In many populous countries such as India, average field size is less than one hectare and the agricultural landscapes are very heterogeneous and covered by a range of

crops and phenological cycles. Further, the soils are highly variable in available nutrients. Often mineral fertilisers have been applied extensively without reference to plant availability and demands resulting in loss of soil fertility and eutrophication of surface waters and sometimes even aquifers. One of the aims of precision agriculture is to avoid the excessive application of chemical nutrients.

A few attempts have been made exploiting the geometrical feature-rich LiDAR point cloud for agricultural applications ([Liu & Bo, 2015](#); [Paulus, Dupuis, Riedel, & Kuhlmann, 2014](#)). These studies have acquired data under controlled laboratory conditions or on a single crop spread over a large area and are of low spatial resolution ([Zhou et al., 2015](#)). Our study has been undertaken to evaluate the potential for plant or patch level information extraction for three different field vegetable crops.

4.1. Crop discrimination at the plant or patch level

The crop discrimination has been approached by considering the object-based classification of the vegetable crops using the dataset generated by the pixel-level fusion of multispectral imagery and LiDAR point cloud and compared with the base datasets independently. The two levels of crop discrimination – the fine classification by N application and the coarse level classification without considering N treatment indicate a new level of opportunity and challenge for remote sensing application to extract plant or patch level information extraction. Compared to the results obtained with LiDAR point cloud, the

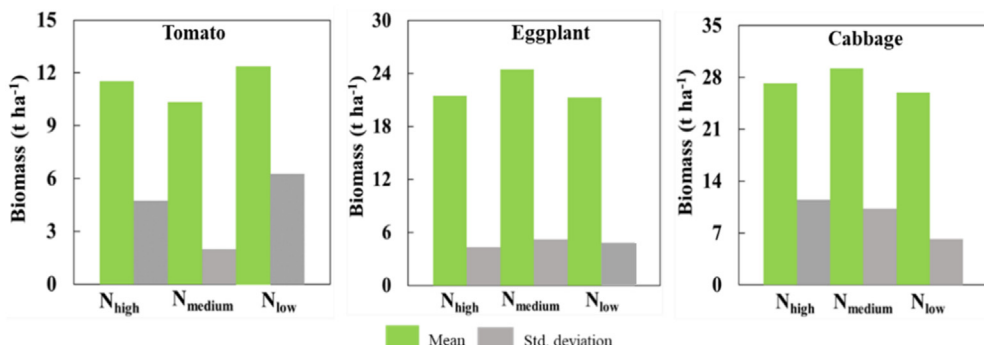


Fig. 19 – First-order statistical representation of the measured biomass across the N treatments of three different vegetables at the experimental station of the University of Agricultural Sciences Bangalore (UASB), GKVK, Campus, India.

quality of crop discrimination from the multispectral imagery, with explicit reference to N treatment, is relatively poor. The highest accuracy of classification is about 72% (from the SVM algorithm; Fig. 6).

Supporting the premise that structural features are vital for crop dissemination at high resolution, the quality of crop discrimination from the fused dataset was very high and consistent across crops and treatments. The best classification accuracy was about 94% (from the SVM algorithm), about 22% higher than the results from multispectral imagery. However, when compared to the best results from the LiDAR point cloud, there is a marginal drop in the accuracy, indicating the possibility of the existence of spectral–structural disorientation for plant level data. This observation indicates the possibility of patch level crop classification by N treatment. The improved results also suggest the complementarity of spectral and geometrical features, thereby illustrating the distinct benefits of fusion of multispectral imagery and LiDAR point cloud for crops mapping. In contrast, the results of the classification of crops without reference to the N treatment indicate a relatively higher accuracy for the multispectral imagery and LiDAR point cloud independently. The difference in accuracy of the classification results from the multispectral imagery and LiDAR point cloud is marginal with 5% variance. However, the accuracy of classification results from the fused dataset show substantial improvement over both base datasets.

Comparison of the classification performance by the algorithm used indicates a distinct pattern. Even though marginal differences are apparent across the datasets, the performance of RF and SVM algorithms is almost similar for the case of classification by N level. For classifications without reference to the N level, the SVM algorithm exhibited substantial underperformance. This may be due to the limited number of training segments viable at the field level when the within-plot plant objects were segments at the broad level. In contrast to the non-parametric decision tree based RF algorithm, the SVM is a statical learning based algorithm which requires a certain level of model-training achievement for stable prediction. Nonetheless, the trend of classification performance was consistent with that of the RF algorithm and the theoretical assumption.

4.2. Biophysical characterisation

The retrieval of two biophysical parameters, plant crown area and biomass, belonging to two distinct categories, showed two different patterns. Due to the destructive harvesting method used for ground measurement of biomass, the number of samples used for validation was limited. In contrast, as is possible without destructive harvesting, the plant crown area has been sampled extensively for ground measurements. The plant height has not been used to compare the results from LiDAR point cloud and multispectral imagery, as plant height is not retrievable from a single date multispectral imagery. The estimates of the plant crown area, a tangible structural parameter, exhibited different correlations with measured values and vary in magnitude and direction based on the data used. When LiDAR point cloud is used for the retrieval, the plant crown area exhibits a close relationship with the

measured values. The estimated values reflect the crop type and N treatment as observed from measured values. For the retrieval from the multispectral imagery, the quality of crown area degraded substantially, and the strength of correlation varied between 65 and 76% of crops with the low and medium N treatments. However, the correlation is relatively poor for the high N treatment. Except for cabbage treated with 'low' N, the estimated values of crown area exhibit substantial overestimations. This also indicated the possibility of soil background and open-canopy gaps in tomato and eggplant, causing some of the pixels filtered out as belonging to non-plant in the image processing stage. The possibility of plant lodging with further skewed spatial spread on the soil also reduced the effective crown area in the purview of the satellite sensor's instantaneous field of view (IFOV). In a recent study, Jayakumari et al. (2021) reported that biomass data under different N levels could be retrieved from multi-temporal LiDAR point clouds with good accuracy. However, acquisitions of multi-temporal data are not practical for any operational intervention of inputs from remote sensing for short duration crops, especially for vegetable crops. In contrast to the substantial performance differences determined from crop classification with and without reference to N, the results from the RF and SVM algorithms for the biophysical parameters estimation are similar for both cases of reference and without reference to N levels (Table 2) across datasets. This suggests the consistency of regression modelling across datasets and levels of N treatment.

The results from the fused dataset exhibit an unusual pattern. On the one hand, the estimates of crown area are consistent and better than the estimates from the multispectral imagery. On the other hand, estimation quality degraded substantially for fused dataset with an estimation error of 20%–28%. This degradation contrasts with the observation that the accuracy of crown area estimation from the LiDAR point cloud is very high and the maximum error of the estimate is about 15%. The reduction in the estimation accuracy with the fused dataset indicates the substantial influence of confused spectral features in modelling the crown area. This observation points out the possibility of destructive interference of spectral and geometrical features for several plant objects, suggesting caution for data fusion applicability.

The estimates of biomass from the three different datasets exhibit a distinct trend compared with the crown area. The LiDAR point cloud has shown the best performance for estimating both the crown area and biomass. Contrasting with the relatively lower performance, estimation accuracy from the fused dataset was substantially higher than the accuracy of estimation from the LiDAR point cloud across crops and N levels. Exhibiting a somewhat similar trend, the accuracy of biomass estimation from the multispectral imagery has also improved substantially, with estimation error of between 10 and 30%. This result also supports the premise that a combination of spectral and geometrical features is vital for plant biophysical descriptions. However, the distinction of biomass estimates by N treatment is unclear for all three datasets. In addition, there are only marginal changes in the accuracy of biomass estimations without direct reference to N treatments. One of the reasons can be ascribed to the field level crop growing conditions and variations in crop growth across

different plots. In addition, heavy Monsoon rains may have caused nutrient transports from one N treatment site to another, influencing the biomass accumulations and degrading the functional limits of the crop growth profile. We recommend more studies on different types of crops, with distinct plant structures and the least exposure to soil background effects.

5. Conclusions

Within-field crop discrimination and biophysical characterisation are vital functions in devising precision agriculture practices. Fusion of data from multispectral and terrain LiDAR sensors offers complementary features for discrimination and biophysical modelling of crops. While maintaining sensitivity to different N levels, the object-based classification of the fused dataset for crop discrimination exhibited a significantly higher accuracy (20%) than the LiDAR point cloud or multispectral satellite imagery. The same trend occurred for crop discrimination without reference N levels. In both cases, the LiDAR point cloud alone to discern crops. For the crown area estimation, the LiDAR point cloud displayed a one-to-one linear correlation with the measured crown area sensitive to N levels with an estimation error of up to 15%. This was also the case for the biomass estimation with LiDAR. For multispectral imagery, the crown area estimation exhibited a moderate correlation partially responsive to N levels. The biomass estimates indicated a strong correlation with the measured ones and were similar to the results obtained from the LiDAR point cloud. For fused datasets, crown area and biomass estimation were well correlated across N levels. Interestingly, the variation observed in the fused dataset was comparable to the LiDAR point cloud indicating the dominance of structural features. The fusion of multispectral and LiDAR point cloud has substantially improved the crop discriminations followed by crown area retrievals, particularly sensible to N levels. However, the accuracy of retrievals from the LiDAR point cloud was also relatively high and consistent. This indicates the dominance of structural features in the fused dataset justifying its performance. Retrieval of biomass, even from the fused dataset, at plant or patch level and sensitivity to N levels is only partially successful. Results highlight the enhanced importance of structural features compared to spectral features for biophysical characterisation of crops.

Declaration of competing interest

The authors declare that they have no known competing financial interests or personal relationships that could have appeared to influence the work reported in this paper.

Acknowledgements

This research has been carried out as part of the Indo-German Research Unit FOR2432 (DBT: The Rural-Urban Interface of Bengaluru-a Space of Transitions in Agriculture, Economics,

and Society) funded by the Department of Biotechnology (DBT), Government of India and the German Research Foundation, Germany. Grants numbers are DBT/IN/German/DFG/14/BVCR/2016, WA 2135/4-1, BU 1308/13-1.

The highly constructive and critical comments and suggestions of anonymous reviewers are gratefully acknowledged.

REFERENCES

- Adam, E., Mutanga, O., Abdel-Rahman, E. M., & Ismail, R. (2014). Estimating standing biomass in papyrus (*Cyperus papyrus L.*) swamp: Exploratory of in situ hyperspectral indices and random forest regression. *International Journal of Remote Sensing*, 35, 693–714.
- Astor, T., Dayananda, S., Nautiyal, S., & Wachendorf, M. (2020). Vegetable crop biomass estimation using hyperspectral and RGB 3D UAV data. *Agronomy*, 10, 1600.
- Axelsson, P. (2000). DEM Generation from laser scanner data using adaptive TIN models. *The International Archives of the Photogrammetry, Remote Sensing*, 23, 110–117.
- Baatz, M., & Schäpe, M. (2000). Multiresolution segmentation – an optimization approach for high quality multi-scale image segmentation. In J. Strobl (Ed.), *Angewandte geographische Informationsverarbeitung XII* (pp. 12–23). Karlsruhe: Wichmann Verlag.
- Belgiu, M., & Drăguț, L. (2016). Random forest in remote sensing: A review of applications and future directions. *ISPRS Journal of Photogrammetry and Remote Sensing*, 114, 24–31.
- Beucher, S., & Meyer, F. (1993). The morphological approach to segmentation: The watershed transformation. In *Mathematical morphology in image processing* (pp. 433–481).
- Blaschke, T. (2010). Object-based image analysis for remote sensing. *ISPRS Journal of Photogrammetry and Remote Sensing*, 65(1), 2–16.
- Breiman, L. (2001). Random forests. *Machine Learning*, 45(1), 5–32.
- Camacho, F., Cernicharo, J., Lacaze, R., Baret, F., & Weiss, M. (2013). GEOV1: LAI, FAPAR essential climate variables and FCOVER global time series capitalizing over existing products. Part 2: Validation and inter comparison with reference products. *Remote Sensing of Environment*, 137, 310–329. <https://doi.org/10.1016/j.rse.2013.02.030>
- Chang, C. C., & Lin, C. J. (2011). LIBSVM: A library for support vector machines. *ACM Transactions on Intelligent Systems and Technology*, 27, 1–27.
- Chao, Z. H., Liu, N., Zhang, P. D., Ying, T. Y., & Song, K. H. (2019). Estimation methods developing with remote sensing information for energy crop biomass: A comparative review. *Biomass and Bioenergy*, 122, 414–425.
- Chhingaryan, A., Sukkarieh, S., & Whelan, B. (2018). Machine learning approaches for crop yield prediction and nitrogen status estimation in precision agriculture: A review. *Computers and Electronics in Agriculture*, 151, 61–69.
- Cortes, C., & Vapnik, V. (1995). Support-vector networks. *Machine Learning*, 20, 273–297.
- Dayananda, S., Astor, T., Wijesingha, J., Chickadibburahalli Thimappa, S., Dimba, C. H., Nidamanuri, R. R., et al. (2019). Multi-temporal monsoon crop biomass estimation using hyperspectral imaging. *Remote Sensing*, 11, 1771.
- Franco, M., & Kelly, C. K. (1998). The interspecific mass-density relationship and plant geometry. *Proceedings of the National Academy of Sciences*, 95, 7830–7835. pmid:9636236.
- Fu, Y. Y., Yang, G. J., Wang, J. H., Song, X. Y., & Feng, H. K. (2014). Winter wheat biomass estimation based on spectral indices, band depth analysis and partial least squares regression using

- hyperspectral measurements. *Computers and Electronics in Agriculture*, 100, 51–59.
- Goodwin, P., & Lawton, R. (1999). On the asymmetry of the symmetric MAPE. *International Journal of Forecasting*, 15, 405–408.
- Guan, Z., Abd-Elrahman, A., Fan, Z., Whitaker, V. M., & Wilkinson, B. (2020). Modeling strawberry biomass and leaf area using object-based analysis of high-resolution images. *ISPRS Journal of Photogrammetry and Remote Sensing*, 163, 171–186.
- Hennessy, A., Clarke, K., & Lewis, M. (2020). Hyperspectral classification of plants: A review of waveband selection generalisability. *Remote Sensing*, 12(1), 113.
- Jayakumari, R., Nidamanuri, R. R., & Ramiya, A. M. (2021). Object-level classification of vegetable crops in 3D LiDAR point cloud using deep learning convolutional neural networks. *Precision Agriculture*, 1–17.
- Jha, S. S., Manohar Kumar, C. V. S. S., & Nidamanuri, R. R. (2021). Flexible atmospheric compensation technique (FACT): A 6S based atmospheric correction scheme for remote sensing data. *Geocarto International*, 36(1), 28–46.
- Kayad, A., Sozzi, M., Gatto, S., Marinello, F., & Pirotti, F. (2019). Monitoring within-field variability of corn yield using sentinel-2 and machine learning techniques. *Remote Sensing*, 11, 2873.
- Kolotii, A., Kussul, N., Shelestov, A., Skakun, S., Yailymov, B., Basarab, R., et al. (2015). Comparison of biophysical and satellite predictors for wheat yield forecasting in Ukraine. *The International Archives of the Photogrammetry, Remote Sensing and Spatial Information Sciences*, 40(7), 39–44.
- Kross, A., McNairn, H., Lapen, D., Sunohara, M., & Champagne, C. (2015). Assessment of rapid eye vegetation indices for estimation of leaf area index and biomass in corn and soybean crops. *International Journal of Applied Earth Observation and Geoinformation*, 34, 235–248.
- Liu, X., & Bo, Y. (2015). Object-based crop species classification based on the combination of airborne hyperspectral images and LiDAR Data. *Remote Sensing*, 7, 922–950.
- Liu, J., Liang, X., Hyppä, J., Yu, X., Lehtomäki, M., Pyörälä, J., et al. (2017). Automated matching of multiple terrestrial laser scans for stem mapping without the use of artificial references. *International Journal of Applied Earth Observation and Geoinformation*, 56, 13–23.
- Li, W., Weiss, M., Waldner, F., Defourny, P., Demarez, V., Morin, D., et al. (2015). A generic algorithm to estimate LAI, FAPAR and FCOVER variables from SPOT4_HRVIR and Landsat sensors: Evaluation of the consistency and comparison with ground measurements. *Remote Sensing*, 7(12), 15494–15516.
- Manzanera, J. A., García-Abril, A., Pascual, C., Tejera, R., Martín-Fernández, S., Tokola, T., et al. (2016). Fusion of airborne LiDAR and multispectral sensors reveals synergic capabilities in forest structure characterization. *GIScience and Remote Sensing*, 53, 723–738.
- Meyer, H., Reudenbach, C., Hengl, T., Katurji, M., & Nauss, T. (2018). Improving performance of spatio-temporal machine learning models using forward feature selection and target-oriented validation. *Environmental Modelling & Software*, 101, 1–9.
- Mhangara, P., Mapurisa, W., & Mudau, N. (2020). Comparison of image fusion techniques using satellite pour l'Observation de la Terre (SPOT) 6 satellite imagery. *Applied Sciences*, 10(5), 1881.
- Neto, A. S., Lopes, D. C., Toledo, J. V., Zolnier, S., & Silva, T. D. (2018). Classification of sugarcane varieties using visible/near infrared spectral reflectance of stalks and multivariate methods. *The Journal of Agricultural Science*, 156(4), 537–546.
- Nidamanuri, R. R., & Zbell, B. (2011). Use of field reflectance data for crop mapping using airborne hyperspectral image. *ISPRS Journal of Photogrammetry and Remote Sensing*, 66, 683–691.
- Nidamanuri, R. R., & Zbell, B. (2013). Understanding the unique spectral signature of winter rape. *Journal of the Indian Society of Remote Sensing*, 41(1), 57–70.
- Otsu, K., Pla, M., Duane, A., Cardil, A., & Brotons, L. (2019). Estimating the threshold of detection on tree crown defoliation using vegetation indices from UAS multispectral imagery. *Drones*, 3, 80.
- Paulus, S., Dupuis, J., Riedel, S., & Kuhlmann, H. (2014). Automated analysis of barley organs using 3D laser scanning: An approach for high throughput phenotyping. *Sensors*, 14(7), 12670–12686.
- Poorter, H., Niklas, K. J., Reich, P. B., Oleksyn, J., Poot, P., & Mommer, L. (2012). Biomass allocation to leaves, stems and roots: meta-analyses of interspecific variation and environmental control. *New Phytologist*, 193(1), 30–50.
- Popescu, S. C., & Wynne, R. H. (2004). Seeing the trees in the forest: Using lidar and multispectral data fusion with local filtering and variable window size for estimating tree height. *Photogrammetric Engineering and Remote Sensing*, 70, 589–604.
- Price, J. C. (1994). How unique are spectral signatures? *Remote Sensing of Environment*, 49(3), 181–186.
- Ramoelo, A., Cho, M. A., Mathieu, R., Madonsela, S., Van de Kerchove, R., Kaszta, Z., et al. (2015). Monitoring grass nutrients and biomass as indicators of rangeland quality and quantity using random forest modelling and WorldView-2 data. *International Journal of Applied Earth Observation and Geoinformation*, 43, 43–54.
- Razaque, A., Ben Haj Frej, M., Almi'ani, M., Alotaibi, M., & Alotaibi, B. (2021). Improved support vector machine enabled radial basis function and linear variants for remote sensing image classification. *Sensors*, 21(13), 4431.
- Shelestov, A., Kolotii, A., Camacho, F., Skakun, S., Kussul, O., Lavreniuk, M., et al. (2015). Mapping of biophysical parameters based on high resolution EO imagery for JECAM test site in Ukraine. In *Geoscience and remote sensing symposium (IGARSS), 2015 IEEE international* (pp. 1733–1736). IEEE.
- Shim, J. Y., & Chang, H. H. (2011). Support vector quantile regression using asymmetric ϵ -insensitive loss function. *Communications for Statistical Applications and Methods*, 18, 165–170.
- Thenkabail, P. S., Lyon, J. G., & Huete, A. (Eds.). (2018). *Biophysical and biochemical characterization and plant species studies*. CRC Press.
- Tong, H., Maxwell, T., Zhang, Y., & Dey, V. (2012). A supervised and fuzzy-based approach to determine optimal multi-resolution image segmentation. *Photogrammetric Engineering and Remote Sensing*, 78(10), 1029–1043.
- Waldner, F., Canto, G. S., & Defourny, P. (2015). Automated annual cropland mapping using knowledge-based temporal features. *ISPRS Journal of Photogrammetry and Remote Sensing*, 110, 1–13.
- Wang, L., Gong, P., & Biging, G. S. (2004). Individual tree-crown delineation and treetop detection in high-spatial-resolution aerial imagery. *Photogrammetric Engineering and Remote Sensing*, 70, 351–357.
- Wang, Y., Wu, G., Deng, L., Tang, Z., Wang, K., Sun, W., et al. (2017). Prediction of aboveground grassland biomass on the Loess Plateau, China, using a random forest algorithm. *Scientific Reports*, 7(1), 1–10.
- Yang, Z. H., Zhang, Y. S., Zheng, T., Lai, W. B., Zou, Z. R., & Zou, B. (2016). Co-registration airborne lidar point cloud data and synchronous digital image registration based on combined adjustment. In *ISPRS international archives of the photogrammetry, remote sensing and spatial information sciences* (Vol. XLI-B1, pp. 259–264).
- Zhou, Z., Huang, J., Wang, J., Zhang, K., Kuang, Z., & Zhong, S. (2015). Object-oriented classification of sugarcane using time-series middle-resolution remote sensing data based on AdaBoost. *PLoS One*, 10(11), Article e0142069.